XXXVI Ibero-Latin American Congress on Computational Methods in Engineering
CILAMCE
Rio de Janeiro, 22-25 Nov 2015

TURBULENCE MODELS COMPARISON IN A FRANCIS TURBINE FLOW SIMULATION: AN APPLIED CASE ON THE ITAIPU TURBINES

João M. Marra

marra@itaipu.gov.br

Itaipu Binacional

Av. Tancredo Neves - 6731, 85866-900, Foz do Iguaçu, Parana, Brazil

Liliana M. Gramani

l.gramani@gmail.com

Federal University of Parana

Av. Cel Francisco Heráclito dos Santos–210, 80210-170, Curitiba, Parana, Brazil

Luiz F. Zubeldia

luiz_zubeldia@hotmail.com

State University of West Parana

Av. Tarquínio Joslin dos Santos -1300, 85870-650, Foz do Iguaçu, Parana, Brazil

Eloy Kaviski

Eloy.dhs@ufpr.br

Federal University of Parana

Jardim das Américas – CEP: 81530-000, Curitiba, Parana, Brazil

Abstract. *The present work shows a comparison between turbulence models, computational mesh and domains, as its ability to numerically modeling the flow in a Francis turbine of Itaipu Hydroelectric Power Plant operating in part load and overload conditions. The main objective of this study is to evaluate the model's ability to predict the amplitude and frequency of pressure pulsations due to the vortices corresponding to each operating condition. In this study were used the SST, k-ε and k-ω turbulence models with three different mesh densities. The results obtained in each simulation were compared with Itaipu data available for these operating conditions. The configuration which results have best adhered to data was used to simulate the entire domain.*

Keywords: *Francis turbine, Turbulence models, CFD, numerical simulation*

1 INTRODUCTION

As farther a hydraulic turbine operates out of its designing conditions, worst is the flow at turbine and greater is the possibility of hydraulic instability phenomena, mainly in turbines with fixed blades runners, as Francis.

Such changes in its operating condition cause pressure fluctuations with damage potential to the physical integrity of the turbine, generating unit and even civil facilities from the powerhouse to the dam.

One cause of this damage is due to the development of vortices at the runner outlet which induce pressure fluctuations which propagate throughout the hydraulic circuit (Alligné, 2011), which may cause dynamic interactions which cause hydraulic instabilities and resonance in the turbine's hydraulic circuit.

To better understand the complex flow in a Francis turbine and evaluate disturbances which occur throughout the hydraulic circuit due to pressure fluctuations can be used the Computational Fluid Dynamics (CFD). For this, knowledge of inherent peculiarities to the application of this technique is extremely important for obtaining satisfactory results. In this work were conducted studies with variation of system's range (domain), spatial discretization (mesh) and turbulence models (SST, k-ε e k-ω) in solving the governing equations of three-dimensional turbulent flow, aiming to evaluate the adopted numerical solver ability of reproducing the hydraulic system behavior as pressure pulsation and associated frequencies to draft tube vortex cores.

Three-dimensional geometric modeling of the entire hydraulic system and numerical simulations were performed using applications of CAD and CFD available at Center for Advanced Studies on Safety of Dams – CEASB considering as object of study the turbines of Itaipu Hydroelectric Powerplant, which one has nominal power of 14,000 MW generated by 20 Francis turbines of 700 MW.

2 GOVERNING EQUATAIONS AND NUMERICAL SOLUTION

Navier-Stokes equations have full capacity to describe the behavior of turbulent flows without needing of additional terms. However, its analytical solution for general cases is still open and, to meet the need of knowing the behavior of fluids in its countless applications, several numeric methods have been developed. (Fox; Mcdonald; Pritchard, 2013).

One of the most successful methods is the Finite Volumes Method, which discretizes differential equations by a conservation balance of each property, e.g., the mass flow for each volume element (Maliska, 2004).

However, turbulent flows of realistic high Reynolds numbers presents a wide range of spatial and temporal turbulence scales which generally involves spatial scales much smaller than the smallest finite volume of a mesh still viable to use. To allow that effects of turbulence be analyzed, a large amount of research in CFD has focused on developing of turbulence models (Ansys, 2013a).

Regarding the numerical solution of the Navier-Stokes equations, is common sense in the scientific world that its direct solution (DNS) is only computationally viable for more simplified systems. Given the inherent difficulty of solution of these equations for real systems, as the flow in the hydraulic system of a turbine Francis, the most widely used alternative is using the Reynolds Averaged Navier-Stokes (RANS) equations. However, due to the required modeling of original equation terms, such procedure represents a filter in the system dynamic response, as demonstrated by Smagorinsky (1963), limiting its application in assessing the dynamic flow behavior. RANS solution modality and other types of solutions of the Navier-Stokes equations will be briefly discussed in the next section, aiming only characterize them.

2.1 Turbulence models

The numerical methods that model the turbulence are grouped into the following three categories:

a) *Reynolds Averaged Navier-Stokes* (RANS) is a method which solves the mean flow and models the effects that all turbulence scales have over the mean flow. (Ansys, 2013a).
b) *Large Eddy Simulation* (LES) is an intermediary methodology that solves the large turbulence scales, which carry most of the energy and models the smaller scales. (Spode, 2006).
c) *Direct Numerical Simulation* (DNS) is able to solve the mean flow and all speed fluctuations due to turbulence. This method is extremely costly in terms of computational resources , so it is not used by the industry to solve flows. (Versteeg; Malalasekera, 2002).

Among these methods, the RANS modeling is preferentially adopted for engineering cases, as it significantly reduces the required computational effort. In this method, the variables in a turbulent flow, e.g., flow velocity, are decomposed in an average term and fluctuating term, as shown in Equation (1). (Davidson, 2011).

$$U_i = \bar{U}_i + u_i \tag{1}$$

The substitution of the average values in the original transport equations results in Reynolds averaged equations given below in index notation, in which the bar indicates the average values, ρ the specific mass, p the pressure, τ_{ij} the stress tensor, S_M the sum of the body forces per unit of volume. *x* and *t* are respectively the spatial and temporal variables.

$$\frac{\partial \rho}{\partial t} + \frac{\partial}{\partial x_j}\left(\rho \bar{U}_j\right) = 0 \tag{2}$$

$$\frac{\partial \rho \bar{U}_i}{\partial_t} + \frac{\partial}{\partial x_j}\left(\rho \bar{U}_i \bar{U}_j\right) = -\frac{\partial p}{\partial x_i} + \frac{\partial}{\partial x_j}\left(\tau_{ij} - \rho \overline{u_i u_j}\right) + S_M \tag{3}$$

Equation (2) is the continuity equation and the Equation (3) is the conservation of momentum equation, in which appears an additional term, the Reynolds stresses, $\rho\overline{u_i u_j}$. This term represents correlations between the floating speeds and it is one more unknown in the system. (Davidson, 2011). To close the equations system it's necessary a model for the Reynolds tensor.

The eddy viscosity hypothesis, proposed by Boussinesq in 1877, establishes that the Reynolds tensor is proportional to the mean velocity gradient, mathematically analogous to the stress and strain tensor in a Newtonian fluid. Thus it is given by:

$$-\rho\overline{u_i u_j} = \mu_t \left(\frac{\partial U_i}{\partial x_j} + \frac{\partial U_j}{\partial x_i}\right) - \frac{2}{3}\delta_{ij}\left(\rho k + \frac{\mu_t \partial U_k}{\partial x_k}\right) \tag{4}$$

where μ_t is the eddy viscosity and *k* is the kinetic energy per unit of mass. (Ansys, 2013b).

When applying the hypothesis to Reynolds Averaged Equation for the momentum is obtained the following:

$$\frac{\partial \rho U_i}{\partial t}+\frac{\partial}{\partial x_j}\left(\rho \bar{U}_i \bar{U}_j\right)=-\frac{\partial}{\partial x_i}\left(p+\frac{2}{3}\rho k\right)+\frac{\partial}{\partial x}\left[\mu_{ef}\left(\frac{\partial \bar{U}_i}{\partial x_j}+\frac{\partial \bar{U}_j}{\partial x_i}\right)\right] \tag{5}$$

where μ_{ef} is the effective viscosity composed by molecular (μ) and eddy (μ_t) viscosity, such that:

$$\mu_{ef}=\mu+\mu_t \tag{6}$$

Eddy viscosity models are distinguished by the manner in which they prescribe the eddy viscosity and eddy diffusivity. (Ansys, 2013b).

2.1.1 The k-ε model

As Ansys (2013b), the model k-ε is based on the eddy viscosity hypothesis, previously presented. In this model the following expression relates the eddy viscosity μ_t to the specific turbulent kinetic energy (k) and specific turbulence eddy dissipation rate (ε), where $C_\mu = 0{,}09$ is a constant and ρ the specific mass:

$$\mu_t = C_\mu \rho \frac{k^2}{\varepsilon} \tag{7}$$

The transport equations for the turbulent kinetic energy (Equation 8) and eddy dissipation rate (Equation 9) give the values of k and ε:

$$\frac{\partial(\rho k)}{\partial t}+\frac{\partial}{\partial x_j}\left(\rho U_j k\right)=\frac{\partial}{\partial x_j}\left[\left(\mu+\frac{\mu_t}{\sigma_k}\right)\frac{\partial k}{\partial x_j}\right]+P_k-\rho\varepsilon \tag{8}$$

$$\frac{\partial(\rho \varepsilon)}{\partial t}+\frac{\partial}{\partial x_j}\left(\rho U_j \varepsilon\right)=\frac{\partial}{\partial x_j}\left[\left(\mu+\frac{\mu_t}{\sigma_\varepsilon}\right)\frac{\partial \varepsilon}{\partial x_j}\right]+\frac{\varepsilon}{k}\left(C_{\varepsilon 1}P_k-C_{\varepsilon 2}\rho\varepsilon\right) \tag{9}$$

where $C_{\varepsilon 1} = 1{,}44$, $C_{\varepsilon 2} = 1{,}92$, $\sigma_k = 1{,}0$ and $\sigma_\varepsilon = 1{,}3$ are constants. The term P_k is the production of turbulence due to viscous forces modeled by the following expression:

$$P_k=\mu_t\left(\frac{\partial U_i}{\partial x_j}+\frac{\partial U_j}{\partial x_i}\right)\frac{\partial U_i}{\partial x_j}-\frac{2}{3}\frac{\partial U_k}{\partial x_k}\left(3\mu_t\frac{\partial U_k}{\partial x_k}+\rho k\right) \tag{10}$$

2.1.2 The k-ω model

According to Ansys (2013b), the k-ω model offers as an advantage treatment for calculating low Reynolds numbers near to the wall. Its formulation does not involve nonlinear damping functions as in the k-ε model and is generally more accurate and robust.

In this model it is assumed that the turbulent kinetic energy and the turbulent frequency are related to eddy viscosity by the expression

$$\mu_t = \rho \frac{k}{\omega} \tag{11}$$

Two transport equations are solved, one for the turbulent kinetic energy (Equation 12) and another for the turbulent frequency (Equation 13):

$$\frac{\partial(\rho k)}{\partial t} + \frac{\partial}{\partial x_j}(\rho U_j k) = \frac{\partial}{\partial x_j}\left[\left(\mu + \frac{\mu_t}{\sigma_k}\right)\frac{\partial k}{\partial x_j}\right] + P_k - \beta' \rho k \omega \tag{12}$$

$$\frac{\partial(\rho \omega)}{\partial t} + \frac{\partial}{\partial x_j}(\rho U_j \omega) = \frac{\partial}{\partial x_j}\left[\left(\mu + \frac{\mu_t}{\sigma_\omega}\right)\frac{\partial \omega}{\partial x_j}\right] + \alpha \frac{\omega}{k} P_k - \beta \rho k \omega^2 \tag{13}$$

where the specific mass, ρ, and the mean velocity vector, U, are treated as known quantities and P_k is the is the turbulence production rate given by Equation (10).

The model constants are given by $\beta' = 0.09$, $\alpha = 5/9$, $\beta = 0.075, \sigma_k = 2$ e $\sigma_\omega = 2$. The Reynolds Stress, $-\rho\overline{u_i u_j}$, is an unknown given by Equation (4).

2.1.3 Model *Shear Stress Transport* (SST)

In the free flow region far from the wall, the results obtained with the k-ε model are few influenced by the boundary conditions, however, near to the wall performance is not satisfactory for boundary layers with adverse pressure gradients (Menter, 1992 apud Versteeg; Malalasekera, 2007). To solve this deficiency, a hybrid model was suggested applying a transformation of the k-ε model for the k-ω model in regions near the wall and the k-ε model in completely turbulent regions far from the wall (Menter, 1992a,b, 1994, 1997 apud Versteeg; Malalasekera, 2007).

A complete formulation of the SST model, given below, is extracted from Menter (2003).

$$\frac{\partial(\rho k)}{\partial t} + \frac{\partial}{\partial x_i}(\rho U_i k) = \tilde{P}_k - \beta' \rho k \omega + \frac{\partial}{\partial x_i}\left[(\mu + \sigma_k \mu_t)\frac{\partial k}{\partial x_i}\right] \tag{14}$$

$$\frac{\partial(\rho\omega)}{\partial t} + \frac{\partial(\rho U_i \omega)}{\rho x_i} = \alpha \rho S^2 - \beta \rho \omega^2 + \frac{\partial}{\partial x_i}\left[(\mu + \sigma_{\omega 1}\mu_t)\frac{\partial \omega}{\partial x_i}\right] + 2(1-F_1)\rho\sigma_{\omega 2}\frac{1}{\omega}\frac{\partial k}{\partial x_i}\frac{\partial \omega}{\partial x_i} \tag{15}$$

where the blending function F_1 is defined by:

$$F_1 = \tanh\left\{\left\{min\left[max\left(\frac{\sqrt{k}}{\beta'\omega y}, \frac{500\nu}{y^2\omega}\right), \frac{4\rho\sigma_{\omega 2}k}{CD_{k\omega}y^2}\right]\right\}^4\right\} \tag{16}$$

where y is the distance to the closest wall and

$$CD_{kw} = m\acute{a}x\left(2\rho\sigma_{\omega 2}\frac{1}{\omega}\frac{\partial k}{\partial x_i}\frac{\partial \omega}{\partial x_i}, 10^{-10}\right) \tag{17}$$

The value of F_1 is equal to zero when far from the wall, thus defining the use of k-ε model and becomes unity when inside the boundary layer indicating the use of the k-ω model.

The eddy viscosity is defined by:

$$\mu_t = \frac{a_1 k}{máx(a_1 \omega, SF_2)} \tag{18}$$

where S is the invariant measure of the deformation rate F_2 and is a second blending function defined by:

$$F_2 = tanh\left\{\left[máx\left(\frac{2\sqrt{k}}{\beta' \omega y}, \frac{500\nu}{y^2 \omega}\right)\right]^2\right\} \tag{19}$$

A turbulent energy production limiter is used for SST model to prevent the buildup of turbulence in stagnant regions:

$$P_k = \mu_t \frac{\partial U_i}{\partial x_j}\left(\frac{\partial U_i}{\partial x_j} + \frac{\partial U_j}{\partial x_i}\right) \rightarrow \tilde{P}_k = min(P_k, 10 \cdot \beta' \rho k \omega) \tag{20}$$

All constants are calculated from a combination of constants corresponding to the k-ε model *(F=0)* and the k-ω model *(F=1)* by the general expression

$$\alpha = \alpha_1 F + \alpha_2 (1 - F) \tag{21}$$

where α corresponds to one of the constants to be calculated. The constants for this model are: $\beta' = 0.09,\ \alpha_1 = 5/9,\ \beta_1 = 3/40,\ \sigma_{k1} = 0.85,\ \sigma_{\omega 1} = 0.5,\ \alpha_2 = 0.44,\ \sigma_{k2} = 1,\ \beta_2 = 0.0828,\ \sigma_{\omega 2} = 0.0856.$

3 LOW FREQUENCY PHENOMENA IN SWIRLING FLOW

This section aim to present the origin of low frequency phenomena that happens when a Francis turbine operates out of its optimum flow conditions. This section discusses too the limitation of the satisfactory representation of hydraulic system behavior at these operatives' conditions through RANS numerical solution of governing equations of three dimensional flows using the turbulence models indicated in the previous section.

In its simplest form, the flow in a Francis turbine can be represented by a one dimensional model. Euler equation for hydraulic machines relates the power absorbed by the turbine only with the fluid inlet and outlet conditions in its runner. According to Equation (22) in order to have an optimum efficiency the fluid must enter in the turbine runner without shock with its blades, being tangential to them, and exiting axially ($U_{V2} = 0$), as happen when the turbine flow rate $Q = Q_{ot}$. However, as the Francis turbines have a fixed blades runner and rotate at a constant synchronous speed, whenever the flow in the turbine get away from their optimum conditions the speeds at inlet and outlet may no longer meet the ideal condition, which normally occurs to meet the required power generation adjustment to its demands, as charge dispatches usually practiced.

$$N = \dot{m}(U_{V1} V_1 - U_{V2} V_2) \tag{22}$$

Due to operation outside of optimum conditions the speed at outlet is no longer fully axial, giving rise to tangencies components which swirl the fluid, generating the well known vortices cores at draft tube. These components cause fluctuations in pressure and can produce significant oscillation in the electrical power, as mentioned by Dorfler (2013). This author also mentions that vortices core depends on distribution of the speed field at runner outlet, the geometry of draft tube and the dynamic response of the hydraulic circuit as a whole.

Such behavior can be seen in Figure 1 by the speed triangle at the outlet of the turbine blades for different flow rate, Q, in the turbine. In part load $(Q < Q_{ot})$ and over load $(Q > Q_{ot})$ the tangential component $\vec{U}_{V2}$ is responsible for the rotational effect on the fluid. In ideal condition $(Q = Q_{ot})$ the flow exits axially and this effect does not occur.

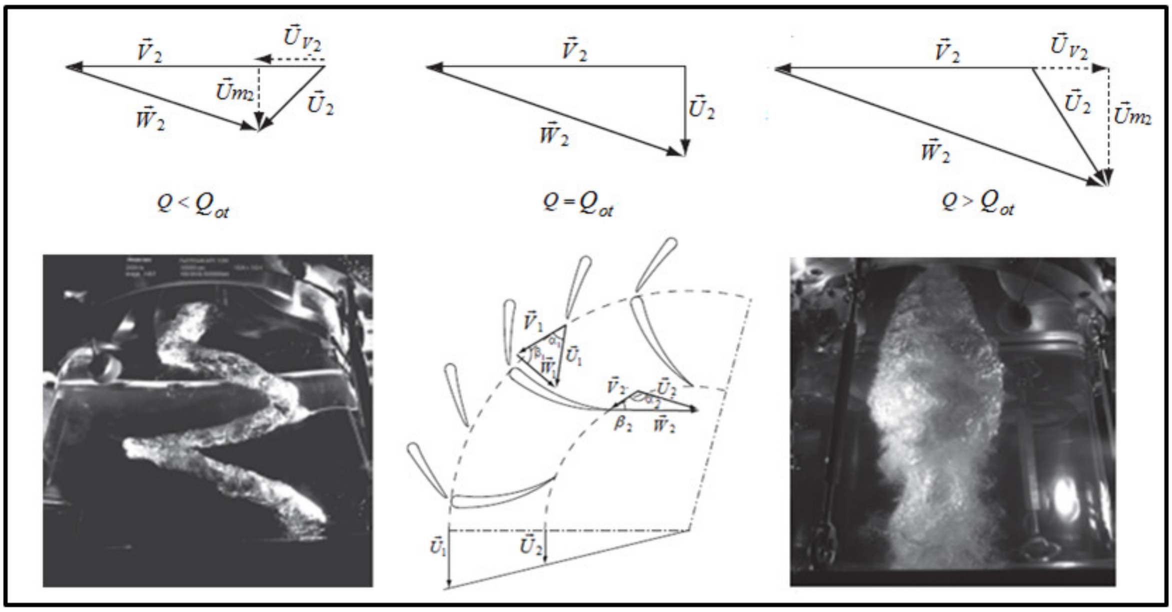

Figure 1. Vortex core (Adapted from Allignė, 2011)

When the boundary conditions allow the occurrence of the water vapor-phase, the vortex core is configured as an underpressure in the core region of the fluid flow. Under these conditions they become visually clear in a transparent draft tube, like the used in reduced models of turbine testing laboratories, as illustrated in Figure 1. These vortices act as an exciter source that dynamically interact with the hydraulic system through a forced oscillation process or a hydraulic instability mechanism. At part load condition the vortex moves like a spiral with precessional movement and acts like a forced vibration with a characteristic frequency. If this frequency coincides with a natural frequency of the system there is a hydraulic resonance situation. At overload condition, the vortex can pulse radially at eigeinvalue frequency of the system, configuring a self-excited phenomenon that produces oscillation even without a forcing source, as explained by Dorfler (2013).

Although the intensity of the rotational component U_{V2} in the fluid has singular importance in pressure fluctuation, other factors such as cavitation, depending on its intensity, also influence this process. The explanation for the effect of cavitation in the pressure pulsation in the draft tube is due to the dynamic gain provided by the resonance with the draft tube fluid system natural frequency, as indicated in the standard IEC 60193 (1999).

To finalize this section, it is observed that single-phase solution of the governing equations (2) and (3) does not allow the appearance of the cavitation, excluding the evaluation of its influence on the hydraulic system behavior. Other limiting factors in the proposed mathematical model are not considering the effects of elasticity and viscoelasticity throughout the whole hydraulic boundary surface and mitigation system of pressure fluctuations by atmospheric aeration or compressed air injection in the turbine.

4 GEOMETRICAL MODELING OF THE HYDRAULIC SYSTEM

The hydraulic system considered as object of study was the existing at Francis turbines of Itaipu Hydroelectric Power Plant, equipped with 20 vertical generating units with the following nominal values for its turbines:

- Shaft power: 715 MW
- Net head: 112.9 mca
- Rotation: 91.6 RPM

The hydraulic system of Itaipu turbine is illustrated in the following figure:

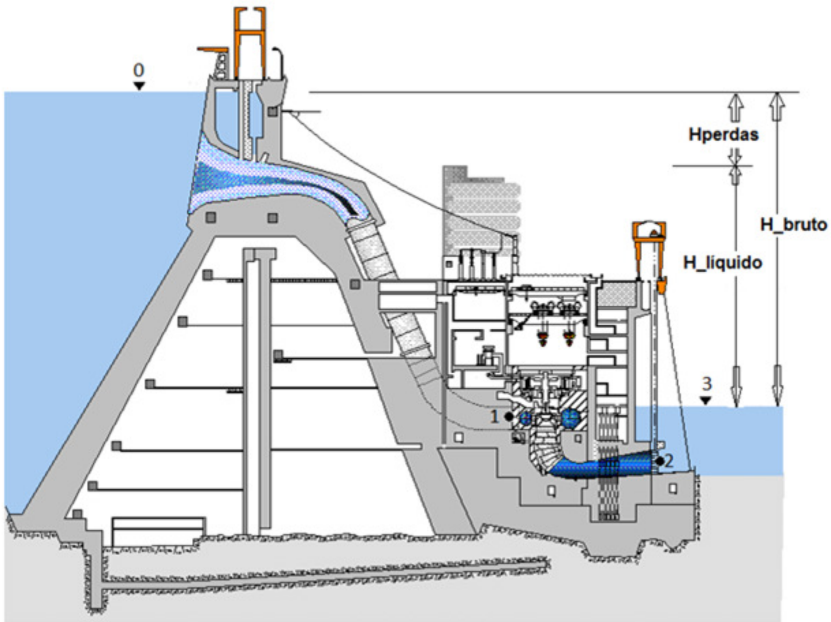

Figure 2. Hydraulic system of Itaipu turbines - Vertical section

The geometrical models used for developing this study were developed based on design's bidimensional technical drawings of the turbine and of the hydraulic system and on some measurements made on site. The models of the set Spiral Case, Pre-distributor, Distributor, Runner and Draft Tube were available at CEASB. The first two geometrical models ones were developed by Vivarelli (2008) and the last one by Borges (2007). Besides these components were also molded geometries of part of the Reservoir, Water Intake and Penstock

4.1 Modeling of stationary domains

4.1.1 Set Spiral Case, Pre-distributor and Distributor

The geometrical models of the set Spiral Case, Pre-distributor and Distributor, for the operating conditions contemplated in this work were developed by Vivarelli (2008). The opening of the distributor is different for each condition and its value is given by the smallest distance between two blades of the Distributor.

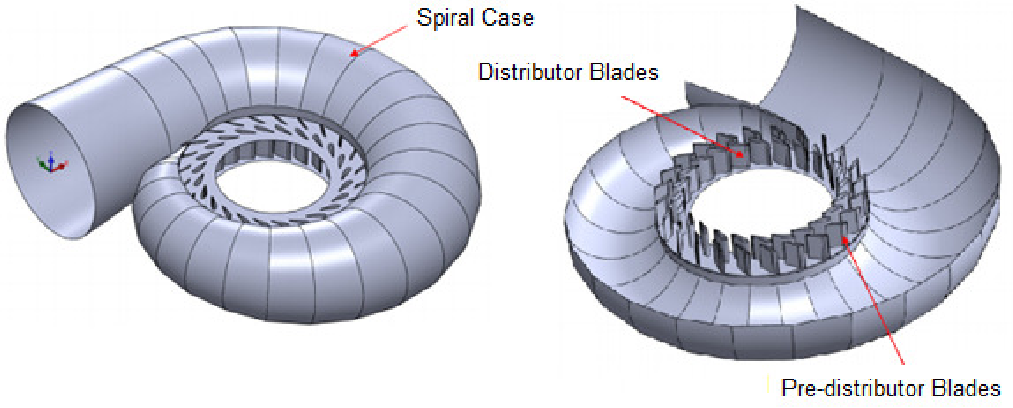

Figure 3. Geometric model of the set Spiral Case, Pre-distributor and Distributor

4.1.2 Draft Tube

The three-dimensional model of the Draf Tube used in this study was developed by Borges (2007). In order to avoid recirculating problems in the outlet region of the draft tube, was introduced an extension to ward off the exit boundary condition, thus making the numerical solution process more stable.

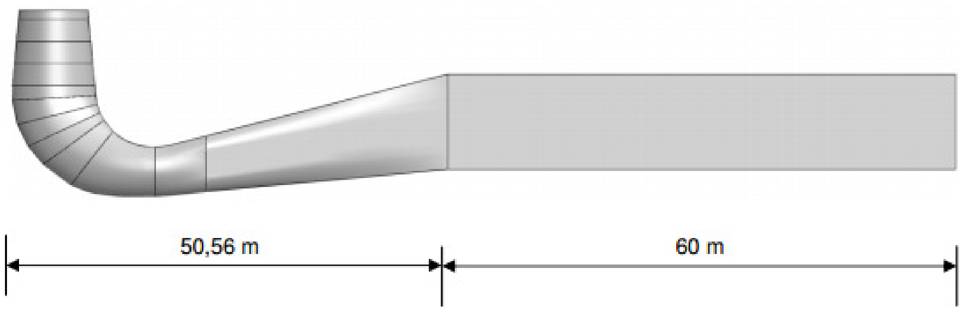

Figure 4. Geometric model of Draft Tube

4.1.3 Resevoir, Water Intake and Penstock

In order to allow evaluation of the influence that presence of components upstream of spiral case has on simulation results, the geometric modeling of the components was made, as illustrated in Figure 5.

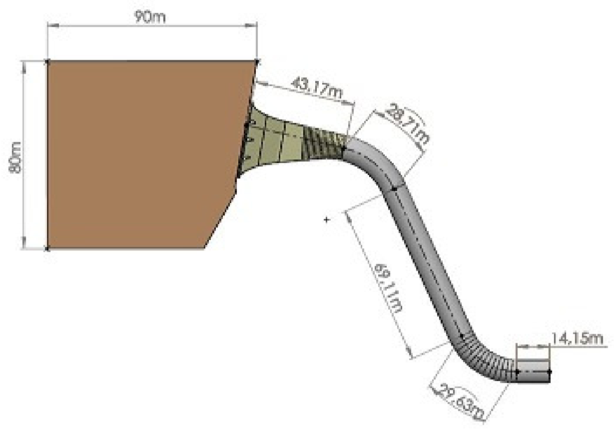

Figure 5. Geometric model of reservoir, water intake and penstock

4.2 Modeling of the rotating domain: the Turbine Runner

The geometric model of the Turbine Runner was developed by Vivarelli (2008). Due to the lack of blade's profile's drawings, was necessary a field survey in order to get points on the blade. The nominal value of the runner outlet diameter is 8.1 m.

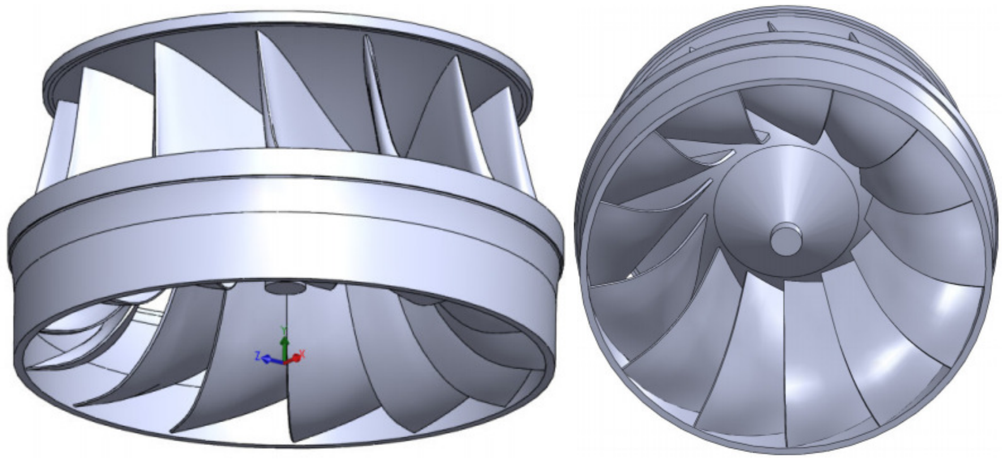

Figure 6. Geometric model of the Turbine Runner

5 BOUNDARY CONDITIONS AND MEASUREMENTS

Aiming more robust results, the boundary conditions chosen were the mass flow at inlet and the static pressure at the outlet of domain. For the domain without the penstock, the inlet boundary condition corresponds to the flow (or speed) at spiral case inlet and the outlet condition corresponds to the static pressure at draft tube outlet. For these conditions, the total pressure is an implicit result of solution.

In order to have an appreciation of the numerical solution of measurements that was developed for two turbine operating points tested in reduced model and prototype, being one for operation with discharge below design point and another with discharge above design point, of which there are images of the vortex core at draft tube of reduced model, as Itaipu (1982). In unitary values, the simulated operating points are:

- Part load: $n_{11} = 65.9\ RPM;\ Q_{11} = 0.580\ m^3/s$
- Over load: $n_{11} = 68.9\ RPM;\ Q_{11} = 0.995\ m^3/s$

The location of these points on the unitary hill chart of reduced model of the turbine and the image of the respective vortex core are shown in Figure 7.

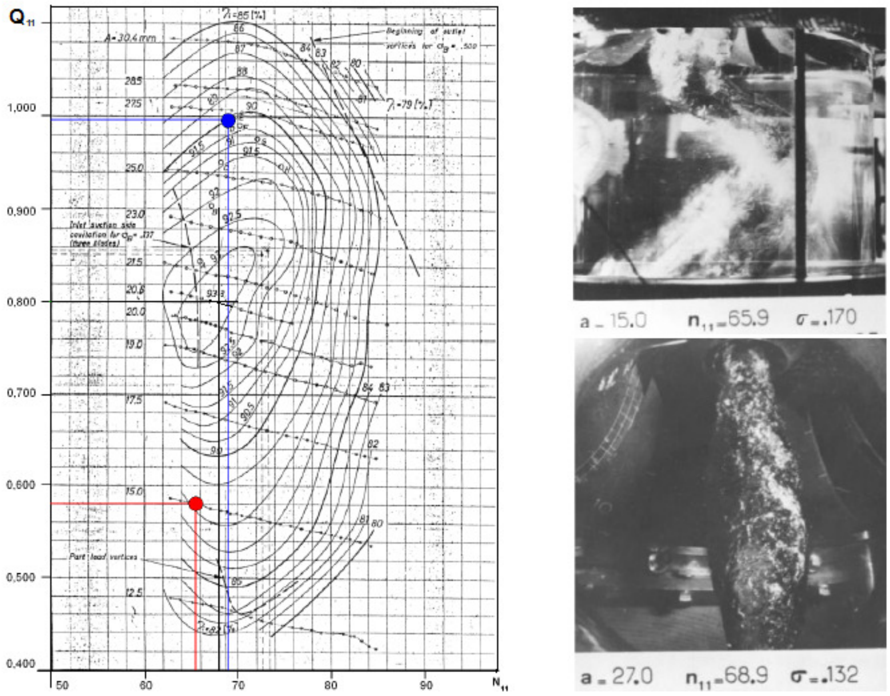

Figure 7. Simulated point and respectives vortex cores (Itaipu, 1982)

Based on the reduced model data (Itaipu, 1982) and measurements made on Hydraulic Stability tests of turbines U04 (Itaipu, 1986) and U11 (Itaipu, 1993) the values considered to evaluate the adherence of numerical simulations are presented in Table 1.

Table 1. Operating parameters and measurements in prototype

Parameters	Part load	Over load
Distributor's opening [%]	49.3	88.8
Net Head [mca]	126.8	116,0
Flow Rate [m^3/s]	434.2	712,4
Efficiency [%]	90.7	94,0
Power [MW]	488.8	760.2
Pressure oscillation at draft tube [$kPa_{p/p}$] – Model	51	6.0
Pressure oscillation at draft tube [$kPa_{p/p}$] – Prototype	90 (U11)	24 (U04)
Pressure oscillation at spiral case [$kPa_{p/p}$] – Prototype	38 (U11)	16 (U04)
Main frequency of the pressure oscillation [Hz]	0.35	1.25

6 NUMERICAL ANALYSIS

6.1 Computational mesh

In order to evaluate the influence the spatial discretization has on the results were tested three meshes with different number of elements for each one of the two evaluated operating conditions. Table 2 shows the total number of elements of the respectives meshes utilized for each simulated condition and also shows the number of elements of the meshes per component of the turbine's domain.

Table 2. Number of elements of the mesh for each simulated condition

	Part Load			Overload		
Component	Mesh 1	Mesh 2	Mesh 3	Mesh 1	Mesh 2	Mesh 3
Spiral Case	1593308	3123673	5356802	1547968	3174044	5226729
Runner	1904397	2593739	3298709	1991912	2510822	3338452
Draft Tube	867022	1652722	4399713	867030	1652722	4398676
Total	4364727	7370134	13055224	4406910	7337588	12963857

A viewing surface of the Mesh 3 is shown in Figure 8, on what the virtual prolongation of draft tube shown in Figure 4 is partially represented.

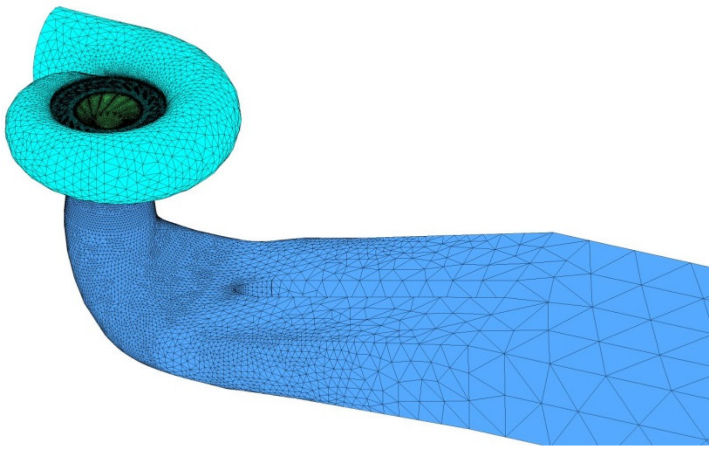

Figure 8. Computational mesh M3

6.2 Temporal discretization, computational resources and simulation times

In order to enhance the convergence of simulations, it was decided to divide them into two stages. The first stage of simulation has the function of providing a good initial condition for the following stage. For this stage was utilized varied time steps, as shown in Table 3, and the first order advection scheme (upwind), which convergence is easier.

Table 3. Time steps used in simulations

Operation Condition	Time Steps [s]	
	Initial stage	Final stage
Part load	20 x 0.01; 20 x 0.1; 20 x 0.01	1440 x 0.00181
Overload	30 x 0.01; 30 x 0.1; 30 x 0.01	1080 x 0.00181

For the second simulation stage was utilized the second order advection scheme and constant time step equivalent to the period that runner takes to rotate one degree. The simulated time for Part Load condition is equivalent to approximately 7,6 runner revolutions and the time for Overload is equivalent to 8,5 revolutions.

The convergence criterion adopted for all simulations was $1x10^{-5}$ to the RMS value of residues.

The computational resources used were a computer with Intel® Xeon® E5-1650 CPU to 3.2GHz processor of which was utilized ten cores, 16GB of RAM and 64-bit operating system Windows 7. The simulation times are shown in Table 4:

Table 4. Simulation time [h]

	Part Load			Overload		
Turbulence Model	Mesh 1	Mesh 2	Mesh 3	Mesh 1	Mesh 2	Mesh 3
SST	18.9	29.2	48.3	11.0	14.3	29
k-ε	17.7	27.8	47.6	9.8	11.7	28.4
k-ω	17.4	27.0	43.1	8.7	13.7	25.9

7 RESULTS

Flow in a Francis turbine operating at Part Load or in Overload produces its characteristics vortex hydraulic phenomena in the flow in draft tube at the turbine runner outlet, as previously mentioned. All these phenomena produce pressure pulsation with a determined amplitude and frequency, being the amplitude strongly dependent of dynamic interaction with entire hydraulic system involved in flow. Monitor points in numerical simulation were inserted at spiral case inlet and at draft tube inlet for acquiring these values at each simulated time step.

7.1 Core vortices prediction

The main flow characteristic in part load and overload is vortices formation at draft tube with a characteristic geometry for each condition, with volume and length dependents of the turbine suction head, that is, of Thoma coefficient, σ.

At the part load condition, all considered turbulence models and meshes were able of reproduce the vortex characteristic shape, but without reaching the expected water vapor pressure for the considered suction head corresponding to σ=0.17. However, the isopressure surfaces indicated at Figure 9, corresponding to the pressure of the suction head considered (300kPa) for this condition, shows a vortex core at turbine output with similar characteristics to the one observed on reduced model test, as available in Itaipu (1982). Below this value, lower is the pressure, the isopressure surfaces obtained at this simulation becomes ever more deformed and divergent of the results of the reduced model test.

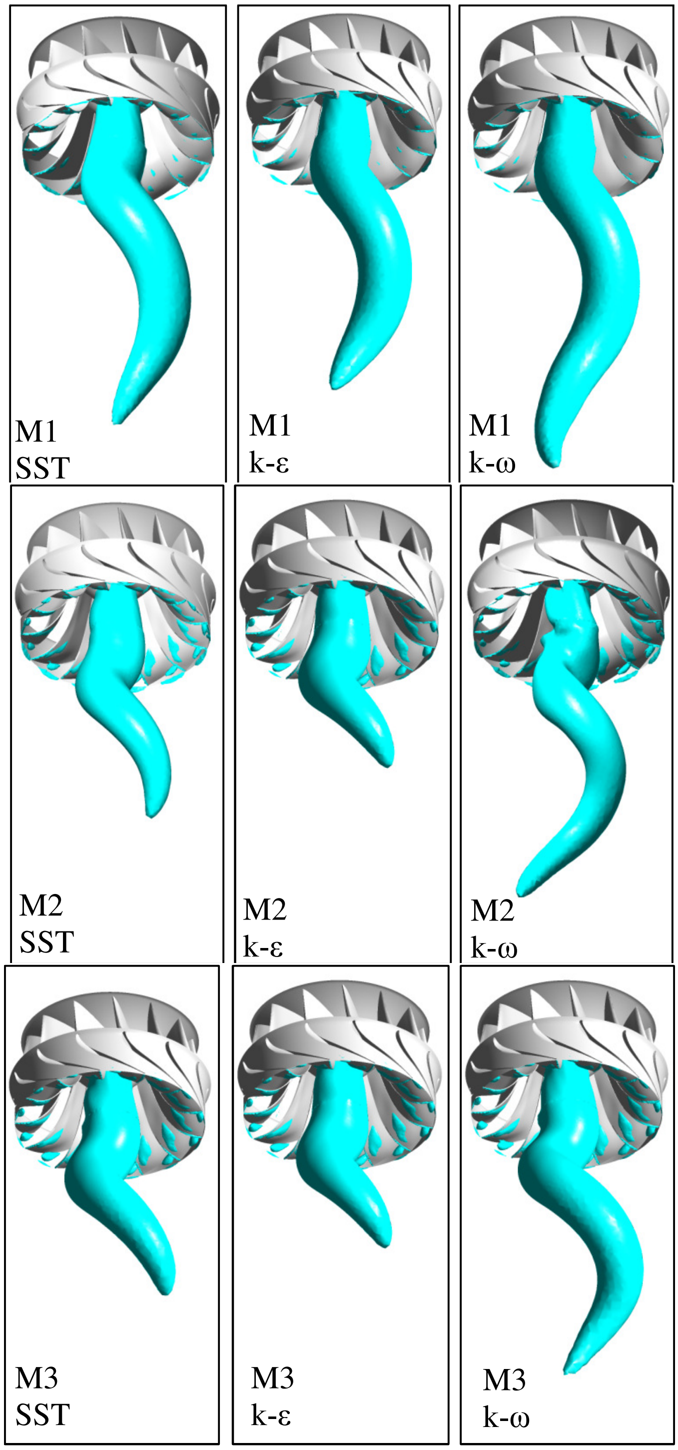

Figure 9. Part Load vortex for each simulated configuration (P = 300 kPa)

For overload condition, the considered turbulence models and meshes were successful in reproducing the characteristic geometry of the vortex of this operative condition and also in reaching the vapor pressure expected for the considered suction head corresponding to σ=0.132, but with very small volume for coarser mesh M1. The effects of turbulence models and mesh refinement can be compared by images shown Figure 10 for isopressure surfaces of 130kPa, wherein the configuration with SST model and mesh M3 presented aspects more adherent to the data available in Itaipu (1982) to this operative condition.

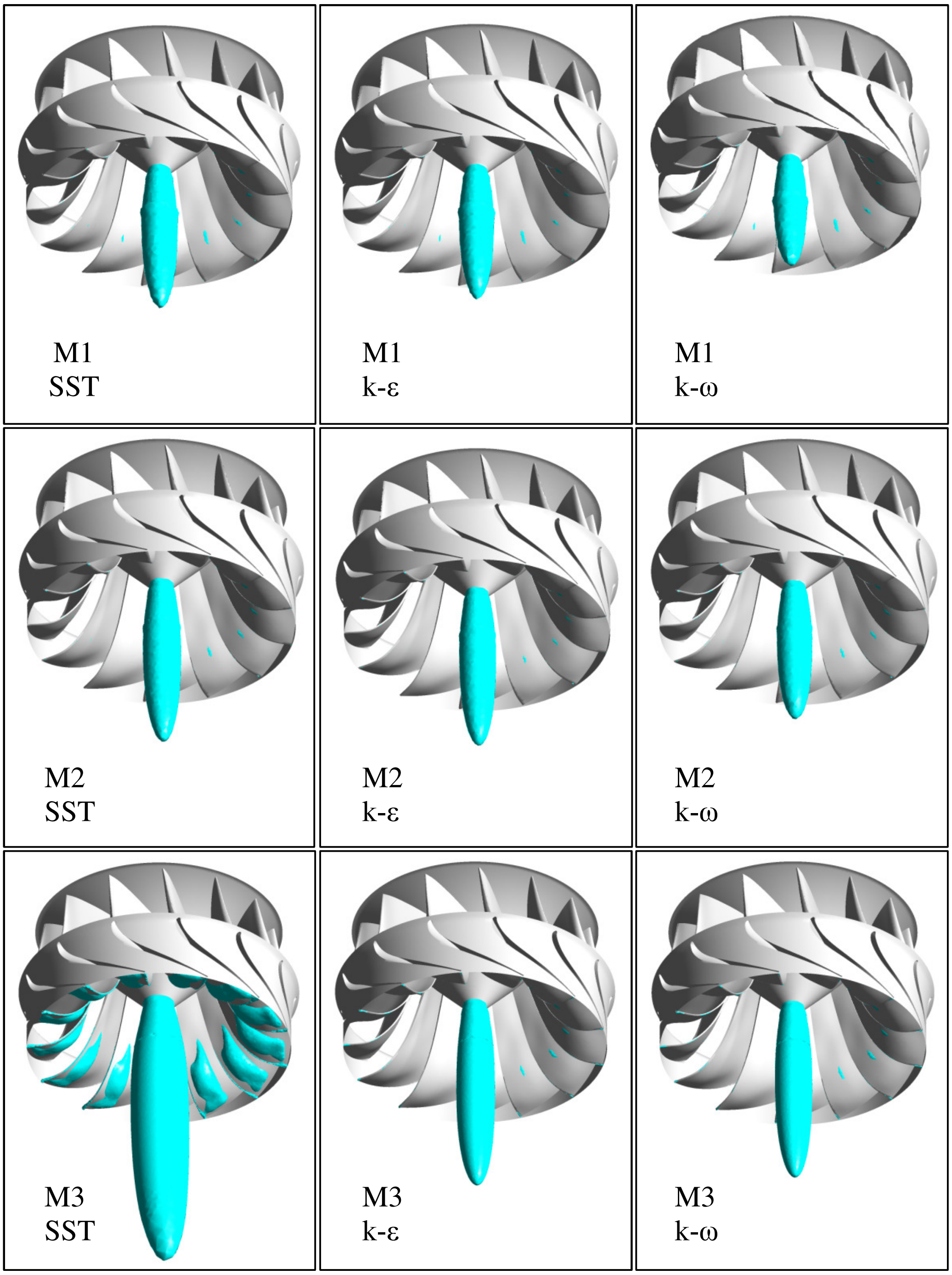

Figure 10. Overload vortices for each simulated configuration (P = 130 kPa)

The vortex volume variation with the reference pressure for isopressure surfaces of 130kPa and vapor pressure (3.2kPa) can be seen at Figure 11 for configuration of mesh and turbulence model M3-SST, where the blue core refers to vapor pressure.

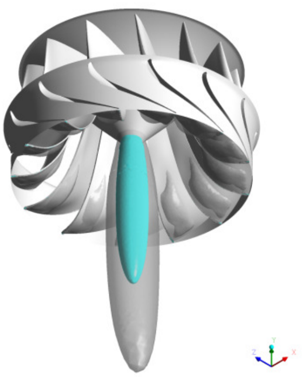

Figure 11. Overload vortices – Volume comparison (P = 130 kPa e P=3.2 kPa)

7.2 Pressure pulsation

The frequency and amplitude of pressure fluctuation due to vortex core presence in numerical simulations were obtained by applying Fast Fourier Transform to temporal values obtained with virtual monitor probe at spiral case and draft tube.

For part load condition, the virtual monitor probe of pressure at draft tube recorded for all simulated configurations the frequency of 0.33Hz, with peak to peak amplitude varying from 34 to 44kPa depending on configuration. As pressure fluctuations caused by vortex propagate to upstream and downstream, disregarding dynamic gains or nonlinearities, as expected, pressure fluctuation at monitor points of spiral case should register the same frequency of draft tube, but with smaller amplitude. This happened for almost all configurations with the exception of two of them (M2 k-ε e M2 k-ω), for which the obtained frequency was 0.16 Hz, as indicated in Table 5.

Other quantities that also indicated adherence of the simulation results to those provided by the reduced model are the values of the generated power and efficiency, whose values expected for part load conditions are 488.8MW and 90.68% respectively.

Table 5. Power, efficiency, pressure pulsation and frequency for part load condition

Parameter	M1 SST	M1 k-ε	M1 k-ω	M2 SST	M2 k-ε	M2 k-ω	M3 SST	M3 k-ε	M3 k-ω
N [MW]	485.7	480.8	484.8	490.4	483.2	491.4	487.3	480.1	487.5
η [%]	90.1	89.2	89.9	90.9	89.6	91.1	90.4	89.1	90.4
ΔH [kPa] (Draft Tube)	40.0	43.9	42.4	35.8	34.7	35.2	36.5	41.7	41.5
f [Hz] (Draft Tube)	0.33	0.33	0.33	0.33	0.33	0.33	0.33	0.33	0.33
ΔH [kPa] (Spiral Case)	13.8	14.7	14.7	12.3	12.9	13.5	15.6	16.9	17.5
f [Hz] (Spiral Case)	0.33	0.33	0.33	0.33	0.16	0.16	0.33	0.33	0.33

Regarding the ability to represent the efficiency, k-ε model had the worst result at all meshes and SST model the best. However, SST and k-ω results present adherent results for the more refined mesh M3.

Regarding overload condition, none of the configuration of simulation for this was able to reproduce vortex dynamic, resulting in an almost static pressure field, therefore, without pressure pulsation, in disagreement to what is observed in the prototype. Notwithstanding, the values obtained for the turbine power and efficiency were satisfactorily adherent to the values predicted by the reduced model transposed to prototype, respectively 760.2MW and 93.97%, mainly for the mesh M1. Meshes M2 and M3 presented worst results for all turbulence models. Table 6 shows the values obtained for the overload simulations.

The obtaining of null pressure fluctuation in overload may be related to the fact that on ITAIPU turbines such fluctuation is due to a hydraulic instability phenomenon. At this situation the single-phase model used for governing equations does not allow the existence of water vapor at the central vortex core, as well as does not consider the elastic and viscoelastic effects of the fluid and the entire hydraulic contour, respectively considered as incompressible and ideally rigid.

Table 6. Power and efficiency of simulated configurations to the overload condition

Parameter	M1 SST	M1 k-ε	M1 k-ω	M2 SST	M2 k-ε	M2 k-ω	M3 SST	M3 k-ε	M3 k-ω
N [MW]	768.5	769.4	767.4	777.9	768.2	775.5	775.9	775.4	773.9
η [%]	94.9	95.1	94.8	96.1	94.9	95.8	95.9	95.8	95.6

7.3 Pressure and velocity fields

Figure 12 displays the streamlines for part load and overload condition. In part load, streamlines allow to distinguish the swirling effect of flow at the same direction of runner's rotation and the flow disequilibrium in the right and left draft tube channels due to tangential component of absolute speed U_{V2} at the same direction of rotation. In overload, is observed a symmetrical concentration of flow at the periphery of the draft tube conical section and elbow, but without disequilibrium of flow in channels.

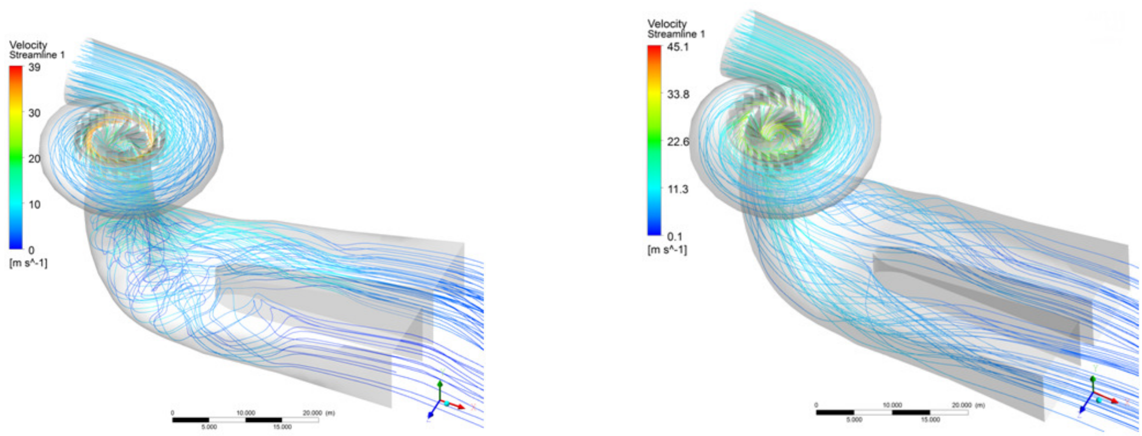

Figure 12. Streamlines for M3 SST - Part load (left) and overload (right)

Figure 13 shows vertical sections of pressure and velocity fields in turbine domain at part load condition. The image corresponding to the pressure field allows visualization of different areas along the pressure transition from spiral case to draft tube, as well as the region corresponding to the spiraled vortex of part load. The image corresponding to velocity field allows observing the velocity transition between the spiral case and the draft tube, denoting the lack of symmetry of velocity field at draft tube due to presence of the spiraled vortex.

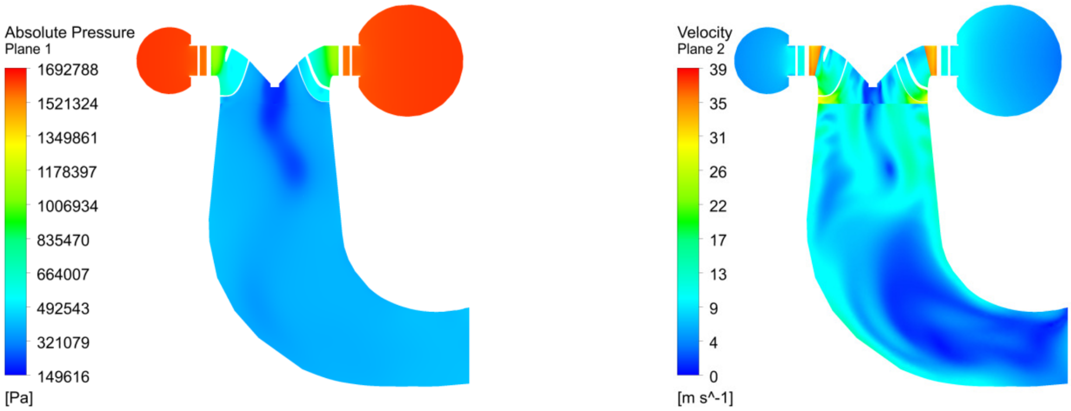

Figure 13. Pressure (left) and velocity (right) fields for M1 SST – Part load

Figure 14 shows vertical sections of the pressure and velocity fields in turbine domain at overload condition. The image corresponding to the pressure field allows visualization of different areas along the pressure transition from spiral case to draft tube, as well as the region corresponding to the oblong shaped vortex core for overload. The image corresponding to velocity field allows observing the velocity transition between the spiral case and the draft tube, denoting the almost symmetry of velocity field at the conical initial stretch of draft tube due to presence of symmetrical vortex core.

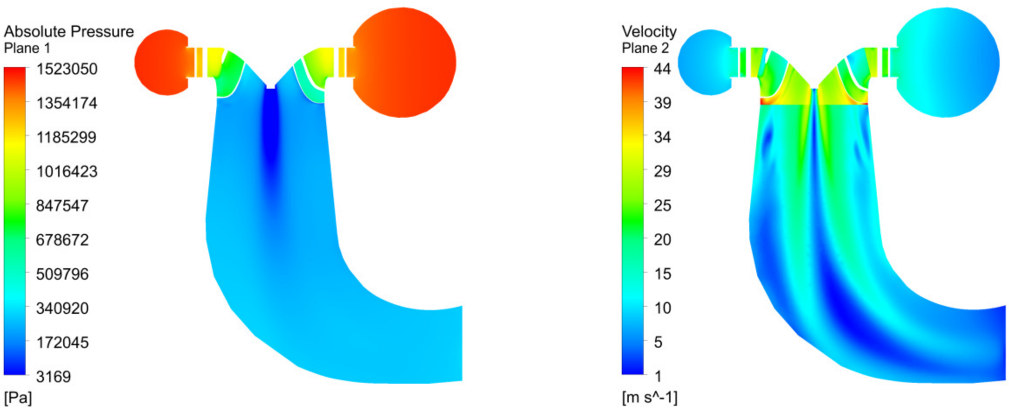

Figure 14. Pressure (left) and velocity (right) for M3 SST – Overload

Considering the topographical difference between the level of downstream and the center of the spiral case inlet section and disregarding the head loss in this stretch, the expected pressure in the spiral case is 1325 kPa. Therefore, is observed a deviation of approximately 368kPa on the expected pressure value for part load condition and of approximately 198kPa for overload condition. This difference is probably due to an insufficient spatial discretization, which is directly influencing the integration process of viscous friction in solving governing equations.

8 FINAL CONSIDERATIONS

All the used configurations of turbulence models and mesh satisfactorily represented the shape and frequency of part load vortex. However, it not allows reaching the vapor pressure at vortex core. The pressure pulsation amplitude showed a deviation of approximately 140% relative to prototype and 30% relative to reduced model, but the value of pressure pulsation attenuation from draft tube to inlet of spiral case showed similar results to those observed in prototype, that is, about 150% for both conditions considered, part load and overload. Part of pressure pulsation results deviation in relation to values of prototype is due to participation of harmonic content in the prototype pressure signal, whereas in numerical results and reduced model the pressure is a signal with only one (main) frequency.

All the used configurations of turbulence models and mesh satisfactorily represented the vortex shape at overload condition and allowed to reach vapor pressure at vortex core. Nevertheless, the configuration with better adherence to the dimensions of the vortex was M3-SST. The amplitude and frequency of the pressure pulsation were unsatisfactorily represented, since the simulation had not captured the vortex dynamics in overload condition.

It is estimated that deviations of simulation results are mainly related to the representation of the flow by single-phase governing equations, the non-consideration of the real biphasic fluid compressibility and flexibility of the wall contour of the whole hydraulic system.

Aiming to improve the results, authors are developing a new study with three-dimensional biphasic model and with boundary conditions updates through an one-dimensional model which considers the vortex dynamics and the flexibility of hydraulic contour surface, as well as the viscoelastic effects.

ACKNOWLEDGEMENTS

The present work only was possible due to the support of the Center for Advanced Studies on Safety of Dams – CEASB belonging to the Itaipu Technological Park – PTI which especially we thank the availability of computer equipment and application necessary for this work.

REFERENCES

Alligné, S., 2011. *Forced and self oscillations of hydraulic sytems induced by cavitation vortex rope of francis turbines*. Tese de doutorado, Escola Politécnica Federal de Lausana, Suíca.

Ansys, 2013a. *Ansys CFX - Solver modeling guide - Release* 15.0. Ansys Inc.

Ansys, 2013b. *Ansys CFX - Solver theory guide- Release* 15.0. Ansys Inc.

Davidson, 2011. *An Introduction to Turbulence Models.* Chalmers.

Dörfler, P; Mirjam, S; Coutou, A. 2013. *Flow Induced Pulsation and Vibrations in Hydroelectric Machinery: Engineers Guidebook for Planning, Design and Troubleshooting*. Springer.

Fox, R. W.; McDonald A. T.; Pritchard, P. J. 2013. *Introdução à Mecânica dos Fluidos. 7. ed. LTC.*

IEC 60193, 1999. Hydraulic turbines storage pumps and pump-turbines – Model acceptance tests. *International Eletrotechnical Commision.*

Itaipu, 1982. *Model Acceptance Tests*. Technical Report. Itaipu Binacional.

Itaipu, 1986. *Ensaios Dinâmicos – U04*. Relatório Técnico. Itaipu Binacional.

Itaipu, 1993. *Estabilidade Hidráulica – U11*. Relatório Técnico. Itaipu Binacional.

Maliska, C. 2004. Transferência de Calor e Mecânica dos Fluidos Computacional. LTC.

Smagorinsk, j., 1963. General circulation experiments with the primitive equations. *Monthly Weather Review*, n. 91, p. 66.

Versteeg, H.; Malalasekera, W. 2007. *An Introduction to Computational Fluid Dynamics: The Finite Volume Method*. Pearson.